J. Fluid Mech. (2012), *vol.* 708, *pp.* 480–501. © Cambridge University Press 2012
doi:10.1017/jfm.2012.320

Dynamics of gravity–capillary solitary waves in deep water

Zhan Wang[1] **and Paul A. Milewski**[2]†

[1] Department of Mathematics, University of Wisconsin–Madison, Madison WI, 53706, USA
[2] Department of Mathematical Sciences, University of Bath, Bath BA2 7AY, UK

(Received 21 February 2012; revised 28 May 2012; accepted 21 June 2012;
first published online 15 August 2012)

The dynamics of solitary gravity–capillary water waves propagating on the surface of a three-dimensional fluid domain is studied numerically. In order to accurately compute complex time-dependent solutions, we simplify the full potential flow problem by using surface variables and taking a particular cubic truncation possessing a Hamiltonian with desirable properties. This approximation agrees remarkably well with the full equations for the bifurcation curves, wave profiles and the dynamics of solitary waves for a two-dimensional fluid domain, and with higher-order truncations in three dimensions. Fully localized solitary waves are then computed in the three-dimensional problem and the stability and interaction of both line and localized solitary waves are investigated via numerical time integration of the equations. There are many solitary wave branches, indexed by their *finite* energy as their amplitude tends to zero. The dynamics of the solitary waves is complex, involving nonlinear focusing of wavepackets, quasi-elastic collisions, and the generation of propagating, spatially localized, time-periodic structures akin to breathers.

Key words: capillary waves, solitary waves, surface gravity waves

1. Introduction

Deep water gravity–capillary waves are relevant in a range of applications, including the understanding of the generation of waves by wind and the interpretation of satellite remote sensing data (see for example Zhang 1995 and Wright 1978). They have also been used to test the predictions of weak turbulence theory (Falcon, Laroche & Fauve 2007). The study of solitary waves in this regime is of particular theoretical interest since it is only under the joint effects of surface tension and gravity that localized water waves in three dimensions have been found in the water wave problem. Such localized waves have recently been observed in the experiments reported in Cho *et al.* (2011*b*). In the deep water limit, these gravity–capillary (GC) 'wavepacket' solitary waves are of a fundamentally different nature from 'long' solitary waves, which are described approximately by the Korteweg–de Vries (KdV), Kadomtsev–Petviashvilli (KP) and related equations in shallow water. The latter bifurcate from linear waves at zero wavenumber whereas the former bifurcate at a finite wavenumber, and hence their oscillatory nature. These oscillatory solitary waves were seen by Ablowitz & Segur (1979) and Akylas (1993) to be approximately described by solitary wave solutions of

† Email address for correspondence: p.a.milewski@bath.ac.uk

https://doi.org/10.1017/jfm.2012.320 Published online by Cambridge University Press

the focusing nonlinear Schrödinger (NLS) equation, which governs the slowly varying envelope of monochromatic waves. In this regime, Akylas (1993) observed that if the phase speed (the speed of crests of the carrier wave) and the group speed (the speed of the envelope) are equal, the solitary waves of NLS will describe approximately solitary waves in the primitive fluid equations. It is simple to show that at a minimum of the phase speed, group and phase speed coincide, and that this occurs at non-zero wavenumber in GC waves for sufficiently deep water. (The condition is that the Bond number be less than $1/3$, which roughly corresponds to a depth greater than a centimetre in the air–water problem.)

In a two-dimensional fluid domain (corresponding to a one-dimensional free surface and henceforth denoted as the '1D problem'), wavepacket solitary waves were first computed in the full fluid equations by Longuet-Higgins (1989) and by Vanden-Broeck & Dias (1992). In three dimensions (with a two-dimensional free surface, denoted the '2D problem'), the first computations of steady solitary waves were by Părău, Vanden-Broeck & Cooker (2005), with related work by Kim & Akylas (2005) and Milewski (2005) on reduced equations. Due to the highly oscillatory and spatially extended nature of these waves, accurate computations are challenging. Localized waves on a two-dimensional water surface are often called 'lumps', a name carried over from their shallow water counterparts which can be approximated by the localized 'lump' solutions of the KP equation, but we prefer to refer to them as wavepacket solitary waves. (This name seems more appropriate since it differentiates oscillatory solitary waves bifurcating from finite wavenumber from long waves bifurcating from zero wavenumber.) In this paper we focus only on the infinite depth case since, for the air–water interface (and most realistic situations), any GC wave dynamics in a bath deeper than a centimetre is in the infinite depth regime. For an air–water interface, these solitary waves bifurcate from a uniform flow with a carrier wavelength of approximately 1.7 cm and a speed of 23 cm s^{-1}.

The stability and dynamics of GC solitary waves in deep water has only recently been studied. In the 1D problem, Calvo, Yang & Akylas (2002) studied the question of linear stability and Milewski, Vanden-Broeck & Wang (2010) studied the time-dependent evolution of solitary waves (stability and collisions) in full potential flow. In two dimensions, there are far fewer studies. The transverse instability of line solitary waves (solitary waves of the 1D problem trivially extended in the transverse variable) has been considered by Kim & Akylas (2007). Line solitary waves are unstable to transverse perturbations of sufficiently long wavelength. Fully two-dimensional dynamics have been considered by Akers & Milewski (2010) in a one-way simplified model and in a quadratic isotropic model in Akers & Milewski (2009). The main goal of this paper is to study two-dimensional dynamics within a more realistic approximation of the potential flow equations. The simplification that we make is to use surface variables using a Dirichlet-to-Neumann map for the velocity potential and then take a particular cubic truncation similar to that suggested in Kim, Dias & Milewski (2012) and used for one-dimensional time-dependent solutions. The rationale for a cubic truncation is to guarantee at least the same local bifurcation behaviour between the model and full potential flow. One important difference from the model we propose and that of Kim *et al.* (2012) is that we use the full (i.e. untruncated) surface tension term. We find that this results in a considerably better approximation of the full equations at larger amplitudes. The approximation proposed is therefore a simple model that can quantitatively capture small- and moderate-amplitude nonlinear CG solitary wave dynamics – a claim we support with 1D comparisons to full potential flow and 2D comparisons with higher-order truncations.

https://doi.org/10.1017/jfm.2012.320 Published online by Cambridge University Press

The focusing two-dimensional cubic NLS equation is central to the understanding of the existence and stability of these solitary waves. We shall see that this equation can be used to correctly predict the existence and certain instabilities of line and wavepacket solitary waves, but does not capture the larger-amplitude stability characteristics, the asymptotic dynamics of unstable waves or the interaction of solitary waves. (The situation in one dimension is worse, since the NLS does not even capture the instabilities of arbitrarily small waves correctly: see for example Calvo *et al.* 2002 and Milewski *et al.* 2010.)

This paper is structured as follows. In § 2 we briefly present the derivation of the cubic truncation model and discuss what can be learned about the solitary waves from the associated NLS equation. In § 3 we present the numerical results: one-dimensional comparisons between the cubic model and the full problem, followed by two-dimensional bifurcation diagrams and comparisons, stability and collision calculations. Lastly, in § 4 we briefly introduce variations on the cubic model including how forcing, dissipation and finite depth effects should be modelled.

2. Formulation

2.1. *Governing equations*

Consider the three-dimensional free-surface water wave problem under the influence of both gravity and surface tension. Let (x, y) denote the horizontal plane, z the vertical direction and t time. The fluid is assumed to be inviscid and irrotational, and therefore there exists a potential function ϕ such that the fluid velocity $(u, v, w) = (\partial_x\phi, \partial_y\phi, \partial_z\phi)$. If the displacement of the water surface is designated by $z = \eta(x, y, t)$, then the governing equations for water waves read

$$\phi_{xx} + \phi_{yy} + \phi_{zz} = 0 \qquad z < \eta(x, y, t), \tag{2.1}$$

$$(\phi_x, \phi_y, \phi_z) \to 0 \qquad \text{as } z \to -\infty, \tag{2.2}$$

$$\eta_t + \eta_x\phi_x + \eta_y\phi_y - \phi_z = 0 \qquad \text{at } z = \eta(x, y, t), \tag{2.3}$$

$$\phi_t + \frac{1}{2}[\phi_x^2 + \phi_y^2 + \phi_z^2] + g\eta = \frac{\sigma}{\rho}\nabla\cdot\left[\frac{\nabla\eta}{\sqrt{1+|\nabla\eta|^2}}\right] \qquad \text{at } z = \eta(x, y, t), \tag{2.4}$$

where $\nabla = (\partial_x, \partial_y)$ is the horizontal gradient operator, and $\nabla\cdot$ is the corresponding horizontal divergence operator. The constants g, ρ, σ are the acceleration due to gravity, density, and the coefficient of surface tension, respectively. Following Craig & Sulem (1993), who worked in the canonical variables introduced by Zakharov (1968), the kinematic and dynamic boundary conditions (equations (2.3)–(2.4)) can be recast in terms of the free-surface potential $\xi(x, y, t) = \phi(x, y, \eta(x, y, t), t)$, and η as

$$\eta_t = G(\eta)\xi, \tag{2.5}$$

$$\xi_t = \frac{1}{2(1+|\nabla\eta|^2)}[(G(\eta)\xi)^2 - |\nabla\xi|^2 + 2(G(\eta)\xi)\nabla\xi\cdot\nabla\eta - |\nabla\xi|^2|\nabla\eta|^2 + (\nabla\xi\cdot\nabla\eta)^2] - \eta + \nabla\cdot\left[\frac{\nabla\eta}{\sqrt{1+|\nabla\eta|^2}}\right]. \tag{2.6}$$

$G(\eta)$ is a scaled Dirichlet-to-Neumann (DtN) operator yielding the vertical velocity of the free surface. It is defined by $G(\eta)\xi = \phi_z - \phi_x\eta_x - \phi_y\eta_y = \sqrt{1+|\nabla\eta|^2}\,\phi_n$,

https://doi.org/10.1017/jfm.2012.320 Published online by Cambridge University Press

where ϕ_n is the derivative of the potential in the outward normal direction to the free surface and ϕ satisfies (2.1)–(2.2) with $\phi(x, y, \eta(x, y, t), t) = \xi$. These equations have also been non-dimensionalized using a characteristic length scale $L = (\sigma/\rho g)^{1/2}$, a time scale $T = (\sigma/\rho g^3)^{1/4}$, and a resulting velocity scale $V = (\sigma g/\rho)^{1/4}$. In CGS units, $g = 981$ cm s^{-2}, and σ/ρ, the ratio of the surface tension coefficient and density, equals 73.5 cm^3 s^{-2} for water.

2.2. *Expansion and truncation*

Coifman & Meyer (1985) prove that if the L^∞-norm and Lipschitz-norm of η are smaller than a certain constant, then G is an analytic function of η. It follows that the DtN operator can be naturally written in the form of Taylor expansion in η, $G = \sum G_i$. For infinite depth, the first three terms of the Taylor series are given by

$$\begin{aligned} G_0 &= |D|, \\ G_1(\eta) &= D \cdot \eta D - G_0 \eta G_0, \\ G_2(\eta) &= -\tfrac{1}{2}[G_0 \eta^2 |D|^2 + |D|^2 \eta^2 G_0 - 2 G_0 \eta G_0 \eta G_0], \end{aligned}$$

where $D = -\mathrm{i}\nabla$ and $|D| = (-\Delta)^{1/2}$. Substituting the expansion of G into the kinematic and dynamic boundary conditions and truncating to cubic order all terms involving ξ gives the evolution problem

$$\eta_t - |D|\xi = (G_1 + G_2)\xi, \tag{2.7}$$

$$\xi_t + (1 - \Delta)\eta = \nabla \cdot \left[\frac{\nabla \eta}{\sqrt{1 + |\nabla \eta|^2}} - \nabla \eta \right] + \frac{1}{2}[(G_0 \xi)(G_0 \xi - 2 G_0 \eta G_0 \xi - 2\eta \Delta \xi) - |\nabla \xi|^2]. \tag{2.8}$$

This formulation and approximation has reduced the three-dimensional nonlinear water wave problem to a two-dimensional one involving only the variables on the surface, which is computationally reasonably simple. In a doubly periodic setting, each term can be efficiently computed using a pseudospectral method and the fast Fourier transform (FFT). We shall henceforth call this the *cubic model*. It is important to note that the only approximation is in terms involving the velocity potential and that effects intrinsic to the free surface alone are not approximated. Similar computational methods based on series truncations of the DtN operator have been used in a variety of water wave problems (see for example Craig & Sulem 1993) and are summarized in detail by Nicholls (2007). The model we propose is somewhat different since the truncation is not explicitly in the DtN but in the boundary conditions, and it has an exact Hamiltonian formulation (described below), which is not always the case for numerical methods based on DtN series truncations.

For the 1D problem, the full (2.1)–(2.4) can be numerically integrated using a time-dependent conformal map method, and we find (see § 3.2.1) that the cubic truncation is extremely accurate. The next reasonable truncation for this problem, at fifth order, involves substantially more computational resources and does not improve accuracy significantly in either one or two dimensions.

The cubic model can also be obtained from the fourth-order truncation of the kinetic energy part of the Hamiltonian expression of the surface water wave problem written in terms of the surface potential. The total energy of the fluid is the sum of kinetic and

https://doi.org/10.1017/jfm.2012.320 Published online by Cambridge University Press

potential energies,

$$H = \frac{1}{2}\int \mathrm{d}x\,\mathrm{d}y \int_{-\infty}^{\eta} (\phi_x^2 + \phi_y^2 + \phi_z^2)\,\mathrm{d}z + \frac{1}{2}\int \eta^2\,\mathrm{d}x\,\mathrm{d}y + \int \left(\sqrt{1+|\nabla\eta|^2} - 1\right)\mathrm{d}x\,\mathrm{d}y \tag{2.9}$$

and an approximate Hamiltonian can be derived by expanding the energy in powers of the η, ξ. This takes the form

$$H[\eta,\xi] \triangleq \widetilde{H}[\eta,\xi] + O(\eta^3\xi^2),$$
$$\widetilde{H}[\eta,\xi] = \int \frac{1}{2}\xi(G_0 + G_1 + G_2)\xi + \frac{1}{2}\eta^2 + \left(\sqrt{1+|\nabla\eta|^2} - 1\right)\mathrm{d}x\,\mathrm{d}y. \tag{2.10}$$

Equations (2.7) and (2.8) can be expressed in canonical form in the sense of Zakharov (1968):

$$\eta_t = \frac{\delta\widetilde{H}}{\delta\xi}, \quad \xi_t = -\frac{\delta\widetilde{H}}{\delta\eta}. \tag{2.11}$$

The system has further physical conserved quantities, of which mass and momentum,

$$\text{mass} = \int \eta\,\mathrm{d}x\,\mathrm{d}y, \tag{2.12}$$

$$\text{momentum} = \int \xi\nabla\eta\,\mathrm{d}x\,\mathrm{d}y, \tag{2.13}$$

are used to monitor the global accuracy of numerical computations of the cubic model.

2.3. *The nonlinear Schrödinger equation*

Traditionally, weakly nonlinear wavepackets are studied using the resulting cubic nonlinear Schrödinger equation (NLS) for the modulational regime of monochromatic waves. It can be derived by substituting the ansatz

$$\begin{pmatrix}\eta\\ \xi\end{pmatrix} \sim \epsilon \begin{pmatrix}A(X,Y,T)\\ B(X,Y,T)\end{pmatrix} \mathrm{e}^{\mathrm{i}(kx+ly-\omega t)} + \text{c.c.} + \epsilon^2 \begin{pmatrix}\eta_1\\ \xi_1\end{pmatrix} + \epsilon^3 \begin{pmatrix}\eta_2\\ \xi_2\end{pmatrix} + \cdots \tag{2.14}$$

into (2.5), (2.6) and ensuring that the series is well ordered for $t = O(\epsilon^{-2})$. Here $X = \epsilon(x - c_g t)$, $Y = \epsilon y$ and $T = \epsilon^2 t$, where c_g is the group velocity in the wave-propagating direction and 'c.c.' represents the complex conjugate of preceding terms. The wave envelope A can then be found to satisfy the NLS equation (Ablowitz & Segur 1979):

$$\mathrm{i}A_T + \lambda_1 A_{XX} + \lambda_2 A_{YY} = \mu|A|^2 A. \tag{2.15}$$

It is a trivial fact that substituting the same ansatz into the equations (2.7), (2.8) instead yields an NLS equation with identical coefficients, which is the motivation for choosing at least a cubic truncation of the DtN operator. We omit the details of the derivation, and just state the results. Choosing $k = 1, l = 0$ as the carrier wave, the phase and group velocity are equal, with the phase velocity at its minimum, $c_{min} = \sqrt{2}$. All of the waves we consider bifurcate from this point and exist only for $c < c_{min}$.

https://doi.org/10.1017/jfm.2012.320 Published online by Cambridge University Press

The coefficients of NLS are given by

$$\lambda_1 = \frac{\sqrt{2}}{4}, \quad \lambda_2 = \frac{\sqrt{2}}{2}, \quad \mu = -\frac{11}{8}\sqrt{2}. \tag{2.16}$$

The solution to the original system is then as follows:

$$\eta = \epsilon A \mathrm{e}^{\mathrm{i}\Theta} - 2\epsilon^2 A^2 \mathrm{e}^{2\mathrm{i}\Theta} + \cdots + \text{c.c.}, \tag{2.17}$$

$$\xi = -\mathrm{i}\sqrt{2}\epsilon A \mathrm{e}^{\mathrm{i}\Theta} + \mathrm{i}2\sqrt{2}\epsilon^2 A^2 \mathrm{e}^{2\mathrm{i}\Theta} + \cdots + \text{c.c.}, \tag{2.18}$$

where $\Theta = x - \sqrt{2}t$. Since the NLS equation (2.15) is of the elliptic or focusing type with solitary wave solutions in both one and two dimensions, and since the phase and group speed are equal at the chosen carrier wave, one can expect small-amplitude solitary waves bifurcating from a uniform flow. These solitary waves of (2.7) and (2.8) can be approximated by the NLS solitary waves found by solving the elliptic eigenvalue problem for $\rho(x, y)$ and Ω:

$$\Delta\rho + \rho^3 = \Omega\rho, \quad \|\rho\|_\infty = 1, \quad \rho \to 0 \quad \text{at } \infty. \tag{2.19}$$

This is obtained by setting $A = |\mu|^{-1/2}\rho(|\lambda_1|^{-1/2}X, |\lambda_2|^{-1/2}Y)\mathrm{e}^{\mathrm{i}\Omega T}$. Denoting $\Delta c \equiv \sqrt{2} - c$, where c is the wave-propagating speed, then, by the chosen scaling, $\Delta c \sim \Omega\epsilon^2$. The total energy of the gravity–capillary solitary wave bifurcating below the minimum phase speed is then calculated by (2.10).

For the one-dimensional problem (2.19) has the well-known unique focusing NLS soliton, $\rho = \operatorname{sech}(x/\sqrt{2})$, $\Omega = 1/2$, $\int \rho^2 = 2\sqrt{2}$ and thus

$$\|\eta\|_\infty \approx \left|\frac{8}{\mu}\right|^{1/2} (\Delta c)^{1/2} + \left|\frac{8}{\mu}\right| \Delta c, \tag{2.20}$$

$$\widetilde{H} \approx \frac{4|\lambda_1|^{1/2}}{|\mu|} \int \rho^2 \left(\frac{\Delta c}{\Omega}\right)^{1/2} = \frac{2^{23/4}}{11} (\Delta c)^{1/2}. \tag{2.21}$$

For the two-dimensional case of interest here, there are countably many solutions to the problem (2.19) (see Alfimov *et al.* 1990 and references therein), and the first three radially symmetric solutions are shown in figure 1. For the ground state, called the Townes soliton in nonlinear optics (Chiao, Garmire & Townes 1964), $\Omega \approx 0.204$, $\int \rho^2 \approx 11.70$, and, in the present hydrodynamic context,

$$\|\eta\|_\infty \approx \left|\frac{4}{\mu\Omega}\right|^{1/2} (\Delta c)^{1/2} + \left|\frac{4}{\mu\Omega}\right| \Delta c, \tag{2.22}$$

$$\widetilde{H} \approx \frac{4|\lambda_1\lambda_2|^{1/2}}{|\mu|} \int \rho^2 \approx 12.04. \tag{2.23}$$

The details of these computations can be found in Akers & Milewski (2010). An interesting particularity is that the physical energy for two-dimensional wavepacket solitary waves is predicted to tend to a finite value of 12.04 as the amplitude approaches zero, which we shall verify in the cubic model. This is purely a consequence of scaling: the radially symmetric envelope's area is proportional to ϵ^{-2}, exactly countering the effect of decreasing amplitude of the wave whose energy density is ϵ^2. Shallow water lump solutions of KP (a valid approximation when the

https://doi.org/10.1017/jfm.2012.320 Published online by Cambridge University Press

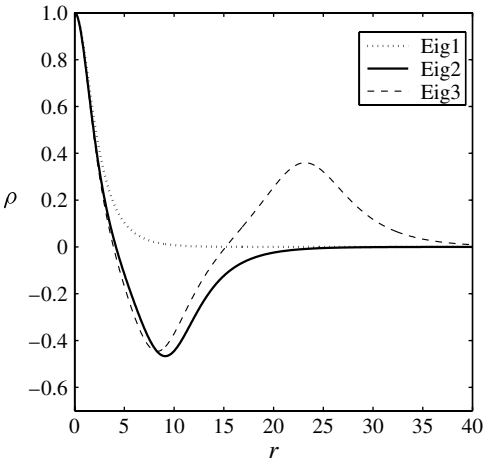


FIGURE 1. First three radially symmetric solutions of (2.19). The corresponding energies of the wavepacket solitary waves for these three envelopes are 12.04, 79.39 and 201.46.

Bond number is greater than 1/3) do not have this property. The higher-energy states of the eigenvalue problem (2.19) can be associated with different families of travelling waves of the cubic model, resulting in a remarkable 'quantization' of the energy of solitary GC waves in the 2D problem.

3. Results

3.1. *Numerical method*

The numerical solution of the cubic model system is implemented on a periodic domain with Fourier pseudospectral methods, where all derivatives and Hilbert transforms are computed in Fourier space with spectral accuracy, while nonlinearities are computed pseudospectrally in real space. The system is first reduced to one complex equation: the Fourier transform of (2.7), (2.8) is

$$\widehat{\eta}_t - |\boldsymbol{k}|\widehat{\xi} = \widehat{N}_1, \tag{3.1}$$

$$\widehat{\xi}_t + (1+\boldsymbol{k}^2)\widehat{\eta} = \widehat{N}_2, \tag{3.2}$$

where the hat indicates the transform operation and $\boldsymbol{k} = (k, l)$ is the transformed variable. With $\mathscr{L}(\boldsymbol{k}) = \sqrt{|\boldsymbol{k}|(1+\boldsymbol{k}^2)}$, the system is rewritten with

$$\widehat{p} = \widehat{\eta} + \mathrm{i}\frac{|\boldsymbol{k}|}{\mathscr{L}}\widehat{\xi}, \quad \widehat{q} = \widehat{\eta} - \mathrm{i}\frac{|\boldsymbol{k}|}{\mathscr{L}}\widehat{\xi}, \tag{3.3}$$

resulting in

$$\widehat{p}_t + \mathrm{i}\mathscr{L}\widehat{p} = \widehat{N}_1 + \mathrm{i}\frac{|\boldsymbol{k}|}{\mathscr{L}}\widehat{N}_2, \tag{3.4}$$

$$\widehat{q}_t - \mathrm{i}\mathscr{L}\widehat{q} = \widehat{N}_1 - \mathrm{i}\frac{|\boldsymbol{k}|}{\mathscr{L}}\widehat{N}_2. \tag{3.5}$$

https://doi.org/10.1017/jfm.2012.320 Published online by Cambridge University Press

Using the fact that ξ and η are real, the two equations are in fact the same, and ξ and η can be recovered from p alone with

$$\widehat{\eta} = \frac{1}{2}\left(\widehat{p}(\boldsymbol{k}) + \widehat{p}\,(-\boldsymbol{k})^*\right), \quad \widehat{\xi} = \frac{1}{2\mathrm{i}}\frac{\mathscr{L}}{|\boldsymbol{k}|}\left(\widehat{p}(\boldsymbol{k}) - \widehat{p}\,(-\boldsymbol{k})^*\right), \tag{3.6}$$

where * indicates complex conjugation. Thus, the problem is reduced to solving

$$\widehat{p}_t + \mathrm{i}\mathscr{L}\widehat{p} = \widehat{N}(p). \tag{3.7}$$

In order to compute travelling waves, we set $\widehat{p}_t = -\mathrm{i}ck\widehat{p}$, and solve the resulting nonlinear algebraic system for the Fourier coefficients using Newton's method. A monochromatic wave modulated by the solution to (2.19) is used as an initial guess. The bifurcation branches are computed via straightforward continuation methods. Time integration of the system is accomplished with a classic fourth-order Runge–Kutta method using an integrating factor (see Milewski & Tabak 1999 for details of both the reduction above and the integrating factor method). The conserved quantities of the system are monitored and in all cases are preserved to a relative error of at most $O(10^{-4})$. All the computations are de-aliased with a doubling of Fourier modes and no filters are used. For two-dimensional computations at least 256×64 modes are used along the propagating and transverse directions respectively. It is often the small-amplitude solutions that are most difficult to compute accurately since the spatial decay of those solutions is much slower. Thus, the computational domain is gradually enlarged as the amplitude becomes smaller.

3.2. *Travelling waves*

3.2.1. *The one-dimensional bifurcation problem and model accuracy*

The bifurcation diagrams of one-dimensional gravity–capillary solitary waves for the full equations in deep water have been presented in Vanden-Broeck & Dias (1992) and others. In figure 2 we compare the speed–amplitude and speed–energy bifurcation diagrams of the cubic model to those of the full equations, the theoretical predictions of NLS and those of a simple one-way model suggested in Akers & Milewski (2009). The amplitude is defined as η at the centre of the wave and the energy is $\widetilde{H}$. The one-way model is given by (in the variables of the present paper)

$$\eta_t + \frac{\sqrt{2}}{2}\eta_x - \frac{\sqrt{2}}{4}\mathscr{H}(\eta - \eta_{xx} - 2\eta_{yy}) - \frac{\sqrt{11}}{4}\eta\eta_x = 0, \tag{3.8}$$

where $\mathscr{H}$ denotes the Hilbert transform in x.

The NLS predictions for $\eta(0)$ as a function of c from (2.17) and (2.21) yield

$$\eta(0) = -\left|\frac{4}{\Omega\mu}\right|^{1/2}(\Delta c)^{1/2} - \left|\frac{4}{\Omega\mu}\right|\Delta c, \quad \eta(0) = \left|\frac{4}{\Omega\mu}\right|^{1/2}(\Delta c)^{1/2} - \left|\frac{4}{\Omega\mu}\right|\Delta c, \tag{3.9}$$

for depression and elevation waves respectively.

From figure 2 we conclude that the cubic model agrees well with the bifurcation picture for the full potential flow equations far beyond the range of validity of the NLS regime, which is quite narrow. Correcting the NLS bifurcation curves with the second harmonic contributions improves the approximation for elevation waves and generally worsens it for depression waves, except in the immediate vicinity of the bifurcation point. The simple one-way model (3.8) restricted to one dimension does as well as NLS (although it has the advantages over NLS in time-dependent dynamics, as discussed in Akers & Milewski 2009). Furthermore, higher-order truncations

https://doi.org/10.1017/jfm.2012.320 Published online by Cambridge University Press

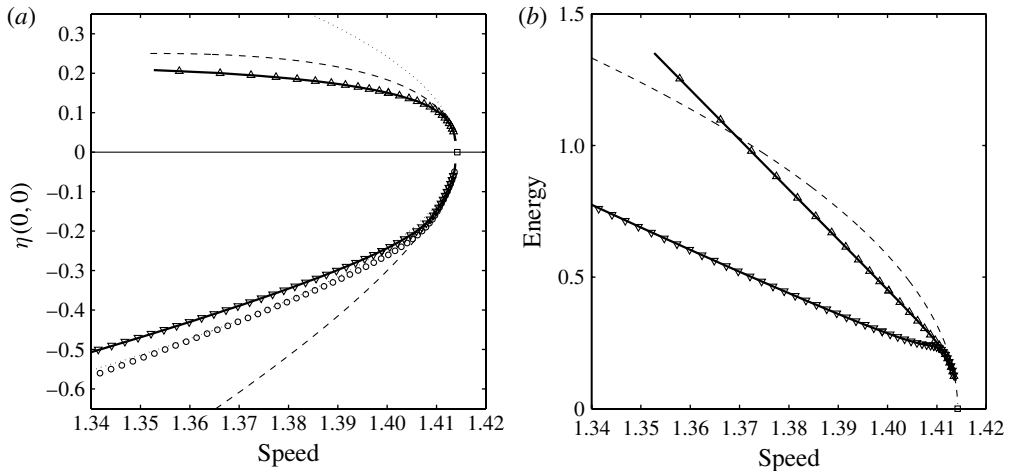


FIGURE 2. (*a*) One-dimensional speed–amplitude bifurcation picture for elevation and depression solitary waves. Solid line, the cubic model; triangles, fully nonlinear potential flow; dotted lines, the leading-order NLS prediction (the first term in (3.9)); dashed lines, the 'corrected' prediction using both terms from (3.9); circles, the simple model (3.8). (*b*) One-dimensional speed–energy bifurcation picture for elevation and depression solitary waves.

do not add appreciable accuracy as shown in figure 3. Even power truncations (i.e. Hamiltonians of odd order) are particularly inaccurate. Typical profiles of the depression and elevation branches of waves are also shown in figure 3. The model is remarkably accurate: at relatively large amplitudes which are far from the NLS regime the relative difference in profile between the full equations and the model are of order 10^{-3} and not visually discernible. Although a quantitative comparison of time-dependent dynamics is involved and beyond the scope of this paper (in particular, methods used to solve the full equations usually do not use a uniform grid in x), we show an example of the inelastic overtaking collision of two solitary waves computed with the full equations (reported in Milewski *et al.* 2010) and the cubic model in figure 4. The results are extremely close, and we see this as further evidence that the cubic model is an accurate representation of the full equations in a broad amplitude range of the CG regime. Comparisons that we have made with the cubic model of Kim *et al.* (2012) show that retaining the full nonlinearity of the surface tension term is far more important (and does not require any more work) than the nonlinearity associated with higher-order corrections of terms involving the velocity potential. Whilst it may be consistent to truncate the surface tension term, it results in a Hamiltonian whose surface tension potential energy is not positive definite.

3.2.2. *The two-dimensional bifurcation problem*

Two-dimensional GC solitary waves of the full equations in infinite depth were first computed in Părău *et al.* (2005) using finite differences and boundary integral methods. Figure 5 shows the bifurcation diagram of GC solitary waves, as obtained from numerical solutions of the cubic model, full potential flow (from a more recent computation performed by Părău and reported in Cho *et al.* 2011*a*), the leading-order and leading-order plus second harmonic of the NLS approximation from (3.9), the model (3.8) and a quintic model following the same truncation method as for our cubic model. In our opinion the potential flow results are under-resolved, particularly

https://doi.org/10.1017/jfm.2012.320 Published online by Cambridge University Press

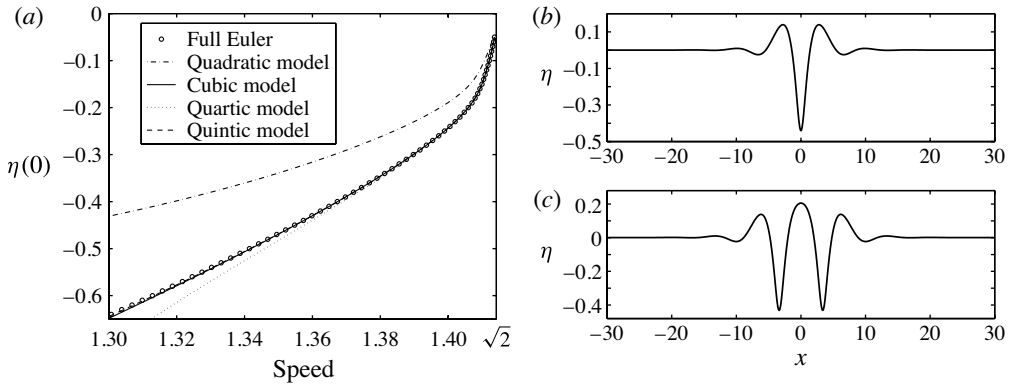


FIGURE 3. (*a*) Comparison of different order truncations for this problem. (*b,c*) Typical free-surface solitary profiles of one-dimensional elevation and depression solitary waves for the cubic model far from the NLS wavepacket regime. (*b*) Depression wave with $\eta(0) = -0.4406$ and $c = 1.3573$. (*c*) Elevation wave with $\eta(0) = 0.2055$ and $c = 1.3579$. The solution to the full equations cannot be visually differentiated from these on this scale. For the depression wave, the maximum difference between the cubic model and full solutions is 6×10^{-4}.

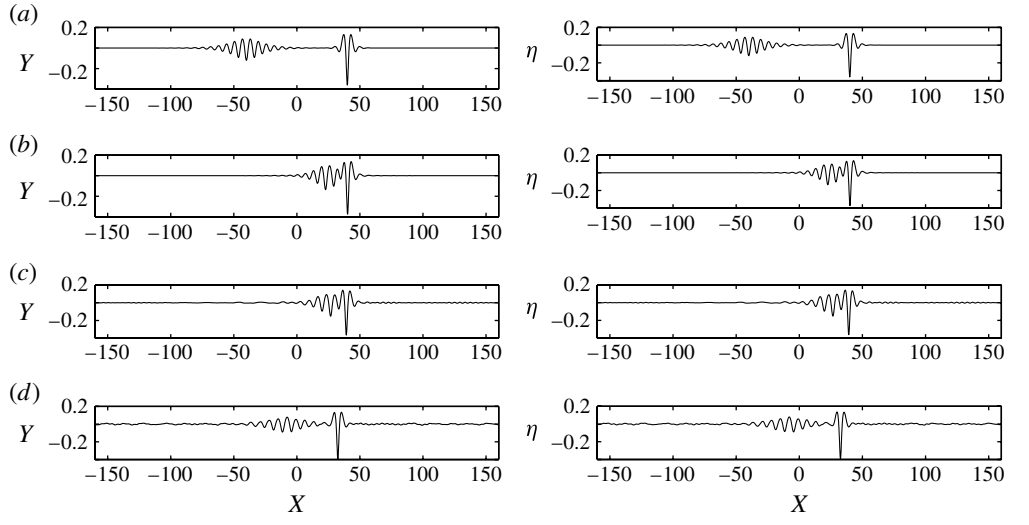


FIGURE 4. Overtaking collision of two depression waves of different amplitudes (minimum free-surface heights of -0.36 and -0.12) shown in a frame of reference moving at the speed of the larger wave. (*a*) $t = 0$, (*b*) $t = 2000$, (*c*) $t = 2500$, (*d*) $t = 3500$. Only the larger wave survives the collision, with the smaller wavepacket to the left of it eventually dispersing. Left, full equations from Milewski *et al.* (2010); right, the cubic model.

at small amplitudes where the waves are highly oscillatory and spatially extended, as they deviate considerably from all other results. This discrepancy between the full potential flow results and the expected amplitudes predicted by NLS had already been noted in Cho *et al.* (2011*a*). We conjecture that the cubic model we present is in quantitative agreement with full potential flow given the accuracy of results at moderate amplitude in the one-dimensional case, and for the two-dimensional case

https://doi.org/10.1017/jfm.2012.320 Published online by Cambridge University Press

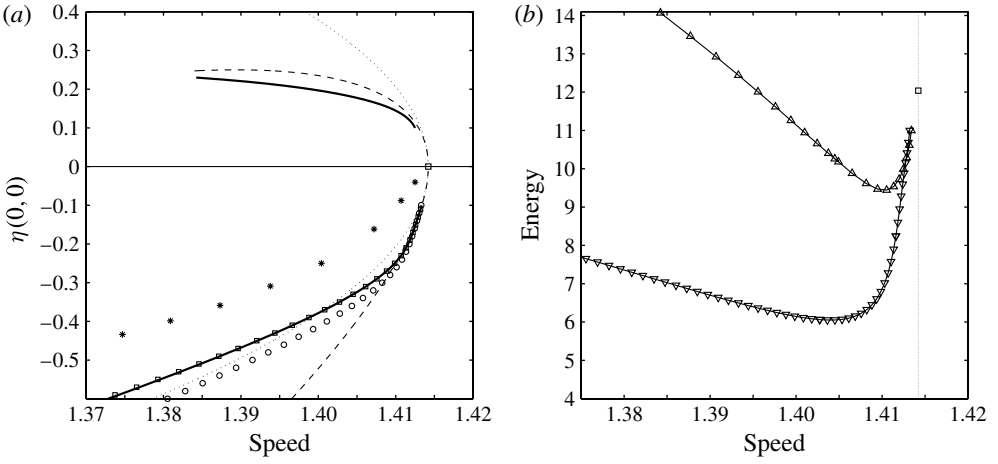


FIGURE 5. (*a*) Speed–amplitude bifurcation curves for elevation and depression two-dimensional solitary waves. Solid line, the cubic model; stars, fully nonlinear potential flow (probably under-resolved: see text); dotted lines, the leading-order NLS prediction (the first term in (3.9)); dashed lines, the 'corrected' prediction using both terms from (3.9); circles, the simple model (3.8); squares, a fifth-order model. (*b*) Speed–energy bifurcation picture for both elevation (triangles pointing up) and depression (triangles pointing down). The bifurcation energy predicted by NLS is indicated by a square.

both the agreement with NLS approximations at small amplitude and the agreement with a fifth-order truncation at moderate amplitude. Furthermore, we note that the cubic model wavepackets have finite energy at their bifurcation point, as predicted by NLS. Typical profiles of the elevation and depression waves corresponding to the bifurcation curves presented in figure 5 are shown in figure 6.

All solutions presented so far are those whose profile envelope at bifurcation is described by the ground state eigenfunction of (2.19). In the 2D problem, we have also computed cubic model solitary wave solutions whose envelope is approximated by radially symmetric higher modes. For example, in figure 12 we show the unstable evolution of the complicated travelling wave resulting from the solitary wave assigned to the second radial mode of (2.19) (the wave is shown in figure 12*a*). This wave has an energy of 79.39 at bifurcation, much higher than the ground state. Non-radially symmetric solutions to (2.19) are discussed in Alfimov *et al.* (1990), but we did not attempt to compute solitary waves whose envelopes are not radially symmetric.

3.3. *Stability, focusing and wave collapse*

There are a few known results that guide us in a numerical study of the two-dimensional stability problem. First, it is known that both depression and elevation plane solitary waves (one-dimensional waves extended in the second dimension) are linearly unstable with respect to sufficiently long small perturbations in the transverse direction. This has been shown both within an NLS approximation Rypdal & Rasmussen (1988) and using arguments based on linearization of the full equations Kim & Akylas (2007). Second, in two dimensions the underlying focusing NLS equation (2.15) is well known to exhibit a finite-time focusing blow-up called wave collapse when, in an unbounded setting, the initial conserved energy $E = \int |\nabla A|^2 - (|A|^4)/2$ is negative (see Zakharov 1972; Sulem & Sulem 1999). (Note that

https://doi.org/10.1017/jfm.2012.320 Published online by Cambridge University Press

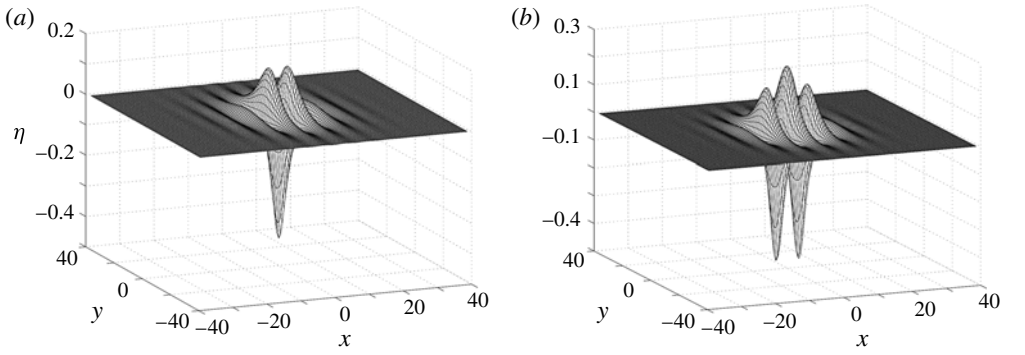


FIGURE 6. (*a*) The depression wavepacket solitary wave solution to the cubic model with $\eta(0,0) = -0.41$ and $c = 1.3907$. (*b*) The elevation wavepacket solitary wave solution to the cubic model with $\eta(0,0) = 0.23$ and $c = 1.3842$.

this energy is not the same one arising from the cubic model.) The result is obtained by a virial argument, whence $M_0 = \int |A|^2$ is conserved and $M_2(t) = \int (X^2 + Y^2)\,|A|^2$ satisfies $M'' = 8E$. Solitary waves which are solutions to the eigenvalue problem (2.19) are critical with $E = 0$. Thus, a small negative energy perturbation leads to focusing and blow-up and a positive energy perturbation leads to spreading of the underlying wave envelope. We thus expect, and will confirm numerically, the instability of localized solitary wave solutions for non-zero envelope energy perturbations in the near-NLS limit of the cubic model (where solitary wave envelopes are well approximated by the NLS). We note that the simple virial argument is not available in a periodic setting (see Sulem & Sulem 1999) but nevertheless seems to predict stability very well in our computations on periodic domains. Third, both elevation and depression wave branches have a critical point in their speed–energy relation (see figure 5), which can lead to an exchange of linear stability of the eigenfunction of the linearized problem associated to the translational invariance symmetry (see for example Akylas & Cho 2008). This is the instability commonly observed in small-amplitude elevation waves of the 1D problem leading to the eventual development of a depression wave (Milewski *et al.* 2010).

All figures of solitary wave dynamics presented are shown with respect to a frame moving with the speed of the wave that was used to construct the initial data. In this frame the main features of the wave evolve slowly.

3.3.1. *Stability of plane waves*

For plane solitary waves, the linear analysis based on NLS (see Akers & Milewski 2010) shows that the transverse perturbation $\mathrm{e}^{\mathrm{i}ly}$ is unstable, when the wavenumber l in the y direction satisfies

$$|l| \lesssim \left|\frac{3\mu}{8\lambda_2}\right|^{1/2} \|u\|_\infty \approx (18)^{1/4}\,(\Delta c)^{1/2} \triangleq l_c. \tag{3.10}$$

We confirm this in our numerical experiments, where a plane solitary wave is perturbed with four transverse perturbations of different wavelengths and the subsequent nonlinear evolution is compared. The perturbation wavenumbers are $l = 1.2l_c$, $1.1l_c$, $0.9l_c$, and $0.8l_c$ respectively. As shown in figure 7, the first two perturbations do not destabilize the plane wave whereas the next two do. The

https://doi.org/10.1017/jfm.2012.320 Published online by Cambridge University Press

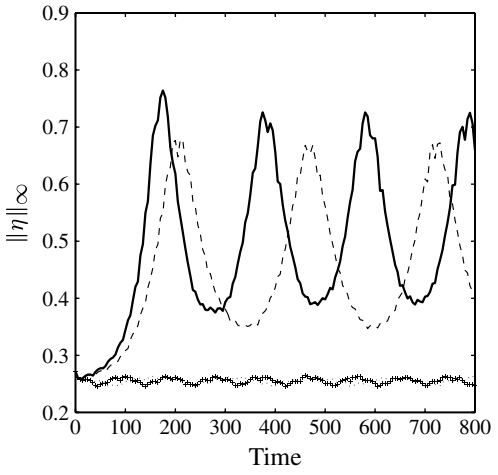


FIGURE 7. Transversal instability of the plane solitary wave, $c = 1.3994$, $\eta(0) = -0.247$. The transverse perturbation is obtained by taking initial data of the form $\eta(x, y, 0) = [1 + 0.1\cos(al_c y)]\widetilde{\eta}(x)$, where $\widetilde{\eta}(x)$ is a travelling wave solution in one dimension, $l_c = 18^{1/4}\Delta c^{1/2}$. Solid line, $a = 0.8$; dashed line, $a = 0.9$; dotted line, $a = 1.1$; plus line, $a = 1.2$.

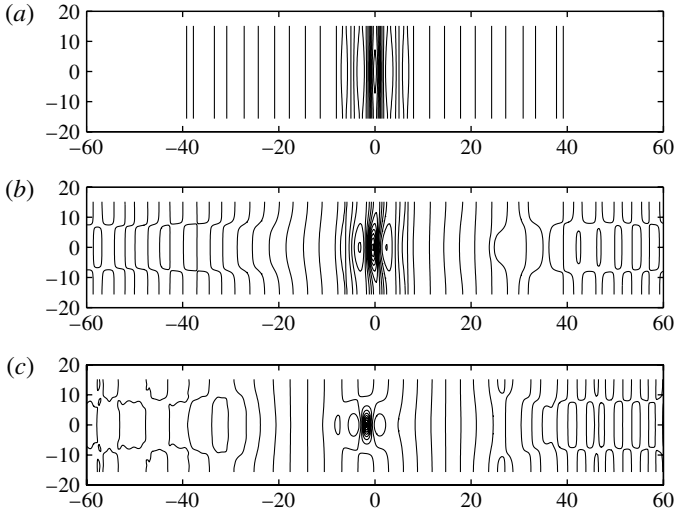


FIGURE 8. Evolution of the transverse instability to a localized solution in the case of $a = 0.8$ in figure 7. The contours are shown at (*a*) $t = 0$, (*b*) $t = 125$, (*c*) $t = 175$.

subsequent evolution of the instability shows a focusing behaviour reminiscent of the underlying collapse dynamics of NLS, as shown in figure 8. This intermediate time focusing is arrested by the generation of a travelling periodically pulsating localized solution similar to a *breather*. A breather is a time-periodic localized structure existing in some integrable systems, including the one-dimensional focusing NLS. Despite our system not being integrable, we shall also call these solutions breathers. In our case, the structure is best described as a localized depression solitary wave with periodic

https://doi.org/10.1017/jfm.2012.320 Published online by Cambridge University Press

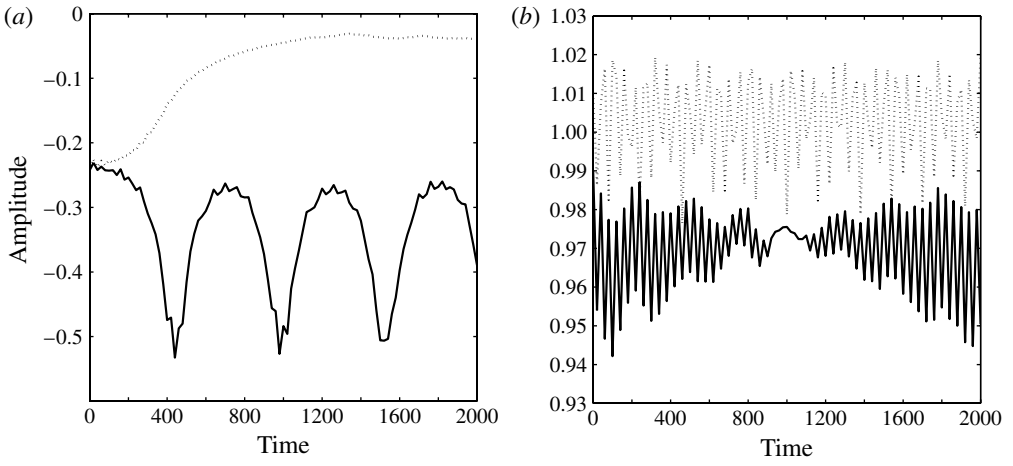


FIGURE 9. (*a*) Evolution of maximum trough depth for perturbed depression waves in the small-amplitude regime ($\eta(0,0) = -0.24$ and $c = 1.4103$). Solid line, negative energy perturbation ($\delta = 0.01$); dashed line, positive energy perturbation ($\delta = -0.01$). (*b*) Evolution of maximum trough depth (normalized by initial maximum trough depth) for depression waves in the moderate-amplitude regime ($\eta(0,0) = -0.49$ and $c = 1.3873$). Solid line, positive energy perturbation ($\delta = 0.01$); dashed line, negative energy perturbation ($\delta = -0.01$).

amplitude modulation, and which appears to be stable (see evolution for $t > 175$ in figure 7) in all our experiments. These breathers are very common and also occur in the nonlinear evolution of instabilities of fully localized solitary waves discussed below.

Throughout our computations, instabilities and wave interactions will invariably lead to some high-frequency dispersive radiation and thus, due to our use of a periodic domain, the remaining coherent structures are embedded in a 'sea' of linear ripples. This is visible in most computations and can also be seen as further evidence of the stability of the resulting structures.

3.3.2. *Stability of localized waves*

The stability of localized travelling waves is considered next. First, the virial argument sketched above implies that near the bifurcation point, both elevation and depression solitary waves are linearly unstable. The virial argument would predict eventual blow-up for negative energy perturbations and this is not observed, in all cases the blow-up is arrested by the generation of a larger-amplitude breather. Dispersive spreading consistent with the envelope spreading predicted by the virial argument is observed for positive energy perturbations. In the computations that we present, we perturb the exact solitary wave solution by a small multiple of itself, by taking initial data $\eta(x, y, 0) = (1 + \delta)\widetilde{\eta}$ where $\widetilde{\eta}$ is the computed travelling wave. Since, for the perturbed wave,

$$E = \int |\nabla A|^2 - \frac{1}{2}|A|^4 \approx -\delta \int |\widetilde{A}|^4, \tag{3.11}$$

where $\widetilde{A}$ is the envelope of the solitary wave, negative energy perturbations correspond to $\delta > 0$ and positive energy ones to $\delta < 0$. In figure 9(*a*) we show the typical

https://doi.org/10.1017/jfm.2012.320 Published online by Cambridge University Press

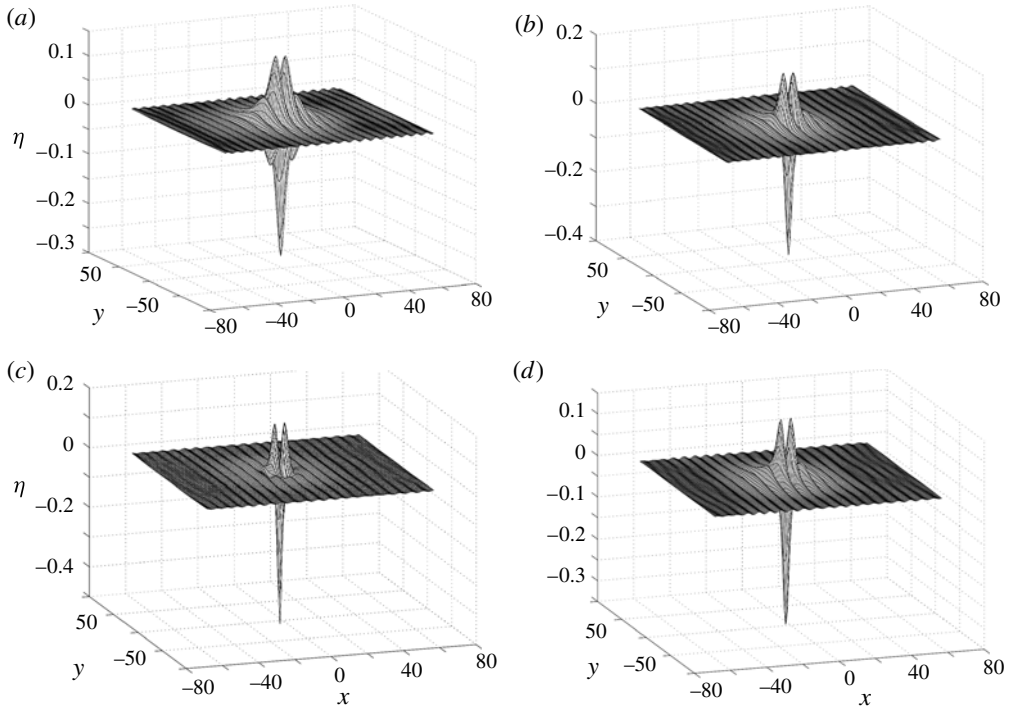


FIGURE 10. Snapshots of one period of a breather taken at (*a*) $t = 1240$, (*b*) $t = 1440$, (*c*) $t = 1520$, (*d*) $t = 1620$ for the small-amplitude negative energy computation discussed in figure 9.

evolution of the amplitude for a perturbed small-amplitude depression solitary wave. For a negative energy perturbation we see focusing arrested by the formation of a breather, whereas for positive energy the amplitude decreases monotonically as a result of dispersive spreading. The case shown is for a depression wave, but the elevation wave dynamics is broadly similar. In figure 10 we show four snapshots of the breather evolution resulting from the unstable small-amplitude depression wave at later times.

For a large class of problems, linear stability may change at a critical point of $H(c)$, the speed–energy curve. This necessary condition for instability was observed by Saffman (1985) for gravity waves, and has since been extended to many other situations. Akylas & Cho (2008) present an application of this result to a wavepacket solitary wave in a model equation. In the present problem, both depression and elevation waves have critical points in $H(c)$. We call solitary waves with speed lower than this critical speed 'moderate-amplitude' and those with higher speed 'small-amplitude', since in all our computations amplitude is a monotonic function of speed. The bifurcation diagram and linear stability of small-amplitude waves are well described by the NLS equation whereas those of moderate-amplitude waves are not. Our numerical simulations show that for depression waves, the exchange of stability does take place at the minimum point in $H(c)$. The evolution of amplitudes of moderate-amplitude depression waves when subject to perturbations is shown in figure 9(*b*). The waves are stable regardless of the sign of δ. Solitary waves (or breathers that are small perturbations of the solitary waves) propagate in the midst of small linear dispersive waves that have been shed by the perturbed initial data.

https://doi.org/10.1017/jfm.2012.320 Published online by Cambridge University Press

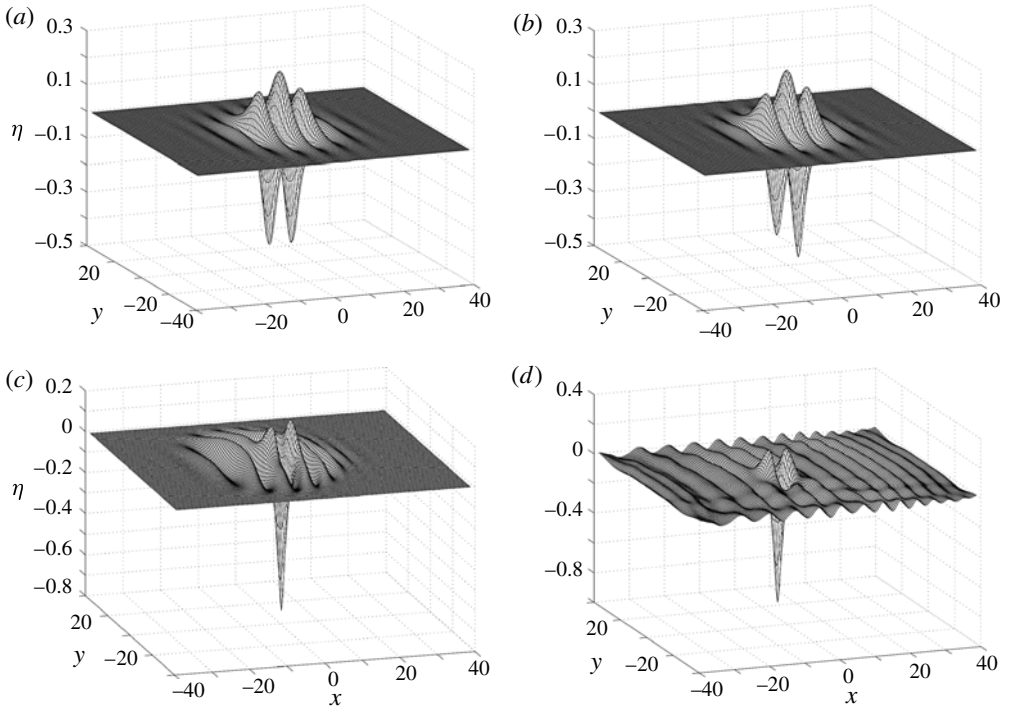


FIGURE 11. Snapshots of the evolution of a moderate-amplitude unstable elevation wave with $\eta(0,0) = 0.2196$, $c = 1.3907$ in the cubic model at (*a*) $t = 0$, (*b*) $t = 120$, (*c*) $t = 200$, (*d*) $t = 270$. The perturbation is 0.01 times the original solitary wave. Some waves are radiated during the transition and the unstable wave evolves into a breather.

All our computations show that elevation waves remain unstable at moderate amplitude. In figure 11 an unstable moderate elevation solitary wave is subject to a small negative energy perturbation and evolves into a depression breather. Similarly, positive energy perturbations will also yield depression breathers, whose energy is much smaller than the elevation waves (see figure 5). The instability is initially similar to that of a one-dimensional depression wave (see Milewski *et al.* 2010): a symmetry breaking whereby the leading trough grows at the expense of the trailing one, and an instability is associated with the translational invariance mentioned above. What follows is collapse focusing, which is arrested by the formation of a depression breather.

From our calculations, we believe there are families of periodic (breather) solutions of different periods and amplitude for each fixed energy above the minimum of the depression solitary waves. The orbits of these breathers in phase space are centred around the fixed point of stable depression solitary waves and may limit to an infinite period solution homoclinic to the unstable depression wave of the same energy. The precise bifurcation diagram for them would require computation of exact periodic localized structures, which is beyond the scope of this paper. A summary of the stability results in this section is shown in table 1.

Lastly, we compute the evolution of a complex solitary wave of the cubic model corresponding to a higher mode of the nonlinear eigenvalue problem discussed previously, and this is shown in figure 12. In this case all perturbations triggered rapid

https://doi.org/10.1017/jfm.2012.320 Published online by Cambridge University Press

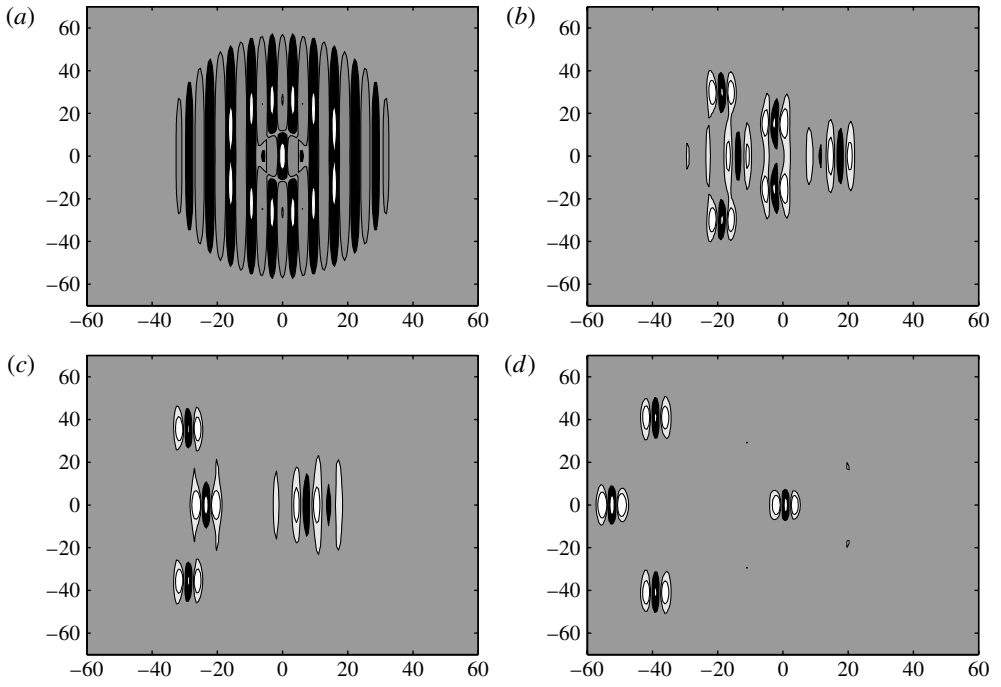


FIGURE 12. Instability of a higher-energy solitary wave with $\eta(0,0) = -0.4028$, $c = 1.4061$. Snapshots of the evolution are shown at (*a*) $t = 0$, (*b*) $t = 800$, (*c*) $t = 1200$, (*d*) $t = 1600$. Four depression breathers emerge from the complex behaviour.

	Positive energy perturbation	Negative energy perturbation
Small depression	Unstable → breather	Unstable → disperses out
Small elevation	Unstable → breather	Unstable → disperses out
Moderate depression	Stable	Stable
Moderate elevation	Unstable → breather	Unstable → breather

TABLE 1. Summary of stability results.

instabilities, but the nonlinear evolution shows a remarkable dynamics with eventual focusing into four depression breathers of different amplitudes.

3.4. *Collisions*

Given the stability of moderate-amplitude depression waves, we have numerically computed their collisions. We have only computed head-on and overtaking collisions of pairs of waves, although in a 2D problem there is a wide range of possible collision scenarios. For head-on collisions, the interaction time between the two waves is insufficient for any strong nonlinear effect to take place and we have only observed very small oscillations that result from the small inelasticity of the collision. The waves essentially traverse each other. The more interesting case is the overtaking collision. Here, the small difference in solitary wave speeds implies that the

https://doi.org/10.1017/jfm.2012.320 Published online by Cambridge University Press

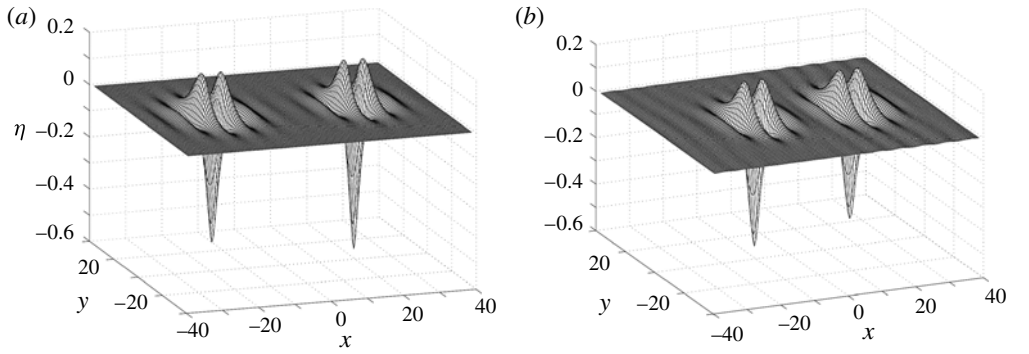


FIGURE 13. Collision of two stable depression solitary waves travelling in the positive x-direction. (a) Initial data consisting of a shifted superposition of two waves with $\eta(0, 0) = -0.56$, $c = 1.3782$ and $\eta(0, 0) = -0.49$, $c = 1.3873$. (b) Solution after interaction at $t = 4000$. Note that the collision is not completely elastic, with the amplitudes decreasing slightly as a result of the collision. The solution was computed in a frame of reference moving at speed 1.3828.

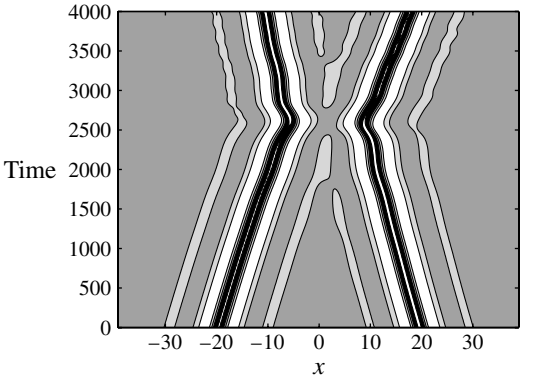


FIGURE 14. Filled contour plot of the centreline of the dynamics $\eta(x, 0, t)$ for the collision reported in figure 13. Note that the wave core remains distant during the collision and that after the collision the waves have exchanged identities and undergone a phase shift.

calculations must be carried out over long times. In the 1D problem collisions were of two types of inelastic collisions (Milewski *et al.* 2010): collisions where both waves survived and collisions where only the larger wave survived when their amplitude difference was large. Here, we have only observed quasi-elastic collisions where both waves survive and the primary effect of the overtaking collision is a rapid and large phase shift of the order of one envelope wavelength. (We do not think that collisions where one wave is destroyed are impossible, especially if both waves are close to the stability threshold, but we have not explored this possibility exhaustively.) Figure 13 shows the before and after free-surface profiles of the waves and figure 14 shows the resulting wave trajectories in (x, t) space. The collisions are weakly inelastic and the wave amplitude is mildly attenuated with some dispersive radiation present during the collision.

https://doi.org/10.1017/jfm.2012.320 Published online by Cambridge University Press

4. Extensions

There are several extensions of the model which, while the detailed study is beyond the scope of this paper, may be useful in studying problems of this type. We have considered fluids of infinite depth only (which in the case of GC flows in water is a good approximation for depths exceeding a few centimetres). If the effect of finite depth is required, the formulation can be modified simply by taking $G_0(\eta) = |D|\tanh(h|D|)$, where h is the mean depth of the fluid normalized by the capillary–gravity length scale and is inversely related to the Bond number. In particular, the shallow water lump dynamics modelled by the Kadomtsev–Petviashvilli (KP) equation should be recovered when the Bond number is greater than $1/3$.

In this paper we have chosen to study the inviscid equations as we believe they have legitimate importance and interest. However, given the small length scales of the waves, it is of practical interest to add the effects of viscosity and forcing when comparing results to experimental data. In the analysis of their experiments, Cho *et al.* (2011*a*) adjusted the simple one-way model proposed in Akers & Milewski (2009) by adding forcing and a viscous damping. The more accurate cubic model can be modified to include small viscous damping effects by using the approximation presented in Dias, Dyachenko & Zakharov (2008), whereby dissipation is modelled through the modification of both kinematic and dynamic boundary conditions:

$$\eta_t - G_0\xi = 2Re^{-1}\Delta\eta + (G_1 + G_2)\xi, \tag{4.1}$$

$$\xi_t + (1-\Delta)\eta = 2Re^{-1}\Delta\xi + P(x,y,t) + \nabla\cdot\left[\frac{\nabla\eta}{\sqrt{1+|\nabla\eta|^2}} - \nabla\eta\right] + \frac{1}{2}[(G_0\xi)(G_0\xi - 2G_0\eta G_0\xi - 2\eta\Delta\xi) - |\nabla\xi|^2]. \tag{4.2}$$

Here, $P(x,y,t)$ is the pressure forcing, and the Reynolds number, which controls the dissipation rate, is given by

$$Re = \frac{VL}{\nu} = \frac{(\sigma/\rho)^{3/4}}{g^{1/4}\nu}, \tag{4.3}$$

where ν is the kinematic viscosity of the fluid. For the case of an air–water interface the Reynolds number of the gravity–capillary wave regime is approximately 400. Since the equations above, when linearized, predict a decay of the solution in times of order $Re/2$, viscous decay is an effect of comparable magnitude to the inviscid time scale of the focusing instability. For air–water, 200 dimensionless time units correspond to approximately 3 s. Under different conditions such as waves on mercury considered in wave turbulence experiments of Falcon *et al.* (2007) or with reduced gravity, the relative effect of viscosity can be further reduced.

For small-amplitude waves, the variation in the transverse direction is not significant compared to that in the propagation direction. One can therefore propose to assume this *a priori*, and simplify the system by deleting all the nonlinear terms which include y-derivatives, obtaining a 'weakly transversal' model which still has the same NLS equation describing wavepackets as the full problem. The Hamiltonian for this model reads

$$\overline{H}[\eta,\xi] = \int \frac{1}{2}\xi(G_0 + \overline{G}_1 + \overline{G}_2)\xi + \frac{1}{2}\eta^2 + \frac{1}{2}\eta_y^2 + \left(\sqrt{1+\eta_x^2}\right)\mathrm{d}x\,\mathrm{d}y, \tag{4.4}$$

https://doi.org/10.1017/jfm.2012.320 Published online by Cambridge University Press

where

$$\overline{G}_0 = (-\partial_{xx})^{1/2}, \tag{4.5a}$$

$$\overline{G}_1 = -\partial_x \eta \partial_x - \overline{G}_0 \eta \overline{G}_0, \tag{4.5b}$$

$$\overline{G}_2 = \tfrac{1}{2}\overline{G}_0 \eta^2 \partial_{xx} + \tfrac{1}{2}\partial_{xx}\eta^2 \overline{G}_0 + \overline{G}_0 \eta \overline{G}_0 \eta \overline{G}_0. \tag{4.5c}$$

Calculations performed with this approximation show excellent agreement with the cubic model at small amplitudes and only qualitative agreement for larger-amplitude solitary waves.

5. Conclusions

The dynamics of gravity–capillary solitary waves on the surface of three-dimensional fluid was studied. The only approximation made was a cubic truncation of terms in the boundary condition arising from the velocity potential, which is equivalent to truncating the Hamiltonian's kinetic energy at fourth order. In two dimensions, where comparisons to the untruncated problem (i.e. fully nonlinear free-surface potential flow) can be accurately measured, this truncation does remarkably well in modelling small- and moderate-amplitude waves. We conjecture that the same is true in three dimensions, and give evidence to support this. It is not clear why a fourth-order kinetic energy is sufficient for this problem, but one may conjecture that the surface tension term's strong regularizing effect on the free-surface displacement graph implies greater accuracy of the truncated approximation throughout the evolution.

In this problem there are undoubtedly infinitely many branches of solitary travelling wave solutions, as this is the prediction of the associated envelope NLS analysis about the bifurcation point. We compute examples of three of them: elevation and depression solitary waves arising from the simplest eigenfunction of the NLS problem and a more complex wave arising from a higher eigenfunction of the same problem. The localized solitary waves have the surprising property that as their amplitude (from peak to trough) decreases to zero as the bifurcation point is approached, their physical energy tends to a finite positive value, quantized by the different eigenfunctions of the NLS equation.

The instability and subsequent evolution for one-dimensional line solitary waves and the various two-dimensional solitary waves have been explored numerically by perturbing the waves and computing the solution through accurate pseudospectral-based methods. All solitary waves are found to be unstable, with the notable exception of moderate-amplitude 'ground state' depression waves. These waves together with travelling breathers, which are periodically oscillating modulations of these travelling states, are (neutrally) stable and appear to be attractors in the long time evolution of the problem. In the dynamics tending to these stable states, dispersive radiation plays the role of dissipation.

The focusing NLS equation adequately predicts the bifurcation and linear stability properties of small-amplitude solitary CG waves. The collapse singularity of initial data, however, is not observed in our computations, leading to the conjecture that an appropriate envelope model for this problem is a cubic–quintic NLS equation where the quintic term is defocusing.

Acknowledgements

We thank Dr E. Părău for making available more resolved numerical results for solitary waves. This work was supported by EPSRC, under grant GR/S47786/01, by

https://doi.org/10.1017/jfm.2012.320 Published online by Cambridge University Press

the Division of Mathematical Sciences of the National Science Foundation, under grant DMS-0908077, and by a Royal Society Wolfson award.

REFERENCES

ABLOWITZ, M. J. & SEGUR, H. 1979 On the evolution of packets of water waves. *J. Fluid Mech.* **92**, 691–715.

AKERS, B. & MILEWSKI, P. A. 2009 A model equation for wavepacket solitary waves arising from capillary–gravity flows. *Stud. Appl. Math.* **122**, 249–274.

AKERS, B. & MILEWSKI, P. A. 2010 Dynamics of three-dimensional gravity–capillary solitary waves in deep water. *SIAM J. Appl. Math.* **70**, 2390–2408.

AKYLAS, T. R. 1993 Envelope solitons with stationary crests. *Phys. Fluids* A **5**, 789–791.

AKYLAS, T. R. & CHO, Y. 2008 On the stability of lumps and wave collapse in water waves. *Phil. Trans. Math. Phys. Engng Sci.* **366**, 2761–2774.

ALFIMOV, G. L., ELEONSKY, V. M., KULAGIN, N. E., LERMAN, L. M. & SILIN, V. P. 1990 On existence of non-trivial solutions for the equation $\Delta u - u + u^3 = 0$. *Physica* D **44**, 168–177.

CALVO, D. C., YANG, T. S. & AKYLAS, T. R. 2002 Stability of steep gravity–capillary waves in deep water. *J. Fluid Mech.* **452**, 123–143.

CHIAO, R. Y., GARMIRE, E. & TOWNES, C. 1964 Self-trapping of optical beams. *Phys. Rev. Lett.* **13**, 479–482.

CHO, Y., DIORIO, J. D., AKYLAS, T. R. & DUNCAN, J. H. 2011*a* Resonantly forced gravity–capillary lumps on deep water. Part 2. Theoretical model. *J. Fluid Mech.* **672**, 288–306.

CHO, Y., DIORIO, J. D., DUNCAN, J. H. & AKYLAS, T. R. 2011*b* Resonantly forced gravity–capillary lumps on deep water. Part 1. Experiments. *J. Fluid Mech.* **672**, 268–387.

COIFMAN, R. & MEYER, Y. 1985 Nonlinear harmonic analysis and analytic dependence. *Proc. Symp. Pure Math.* **43**, 71–78.

CRAIG, W. & SULEM, C. 1993 Numerical simulation of gravity waves. *J. Comput. Phys.* **108**, 73–83.

DIAS, F., DYACHENKO, A. I. & ZAKHAROV, V. E. 2008 Theory of weakly damped free-surface flow: a new formulation based on potential flow solutions. *Phys. Lett.* A **372**, 1297–1302.

FALCON, L., LAROCHE, C. & FAUVE, S. 2007 Observation of gravity–capillary wave turbulence. *Phys. Rev. Lett.* **98**, 094503.

IOOSS, G. & KIRRMANN, P. 1996 Capillary gravity waves on the free surface of an inviscid fluid of infinite depth: existence of solitary waves. *Arch. Rat. Mech. Anal.* **136**, 1–19.

KIM, B. & AKYLAS, T. R. 2005 On gravity–capillary lumps. *J. Fluid Mech.* **540**, 337–351.

KIM, B. & AKYLAS, T. R. 2007 Transverse instability of gravity–capillary solitary waves. *J. Engng Math.* **58**, 167–175.

KIM, B., DIAS, F. & MILEWSKI, P. A. 2012 On weakly nonlinear gravity–capillary solitary waves. Part 1. Bifurcation of solitary wavepackets. *Wave Motion* **49** (2), 221–237.

LONGUET-HIGGINS, M. S. 1989 Capillary–gravity waves of solitary type on deep water. *J. Fluid Mech.* **200**, 451–478.

MILEWSKI, P. A. 2005 Fast communication: three-dimensional localized gravity–capillary waves. *Commun. Math. Sci.* **3**, 89–99.

MILEWSKI, P. A. & TABAK, E. G. 1999 A pseudospectral procedure for the solution of nonlinear wave equations with examples from free-surface flows. *SIAM J. Sci. Comput.* **21** (3), 1102–1114.

MILEWSKI, P. A., VANDEN-BROECK, J.-M. & WANG, Z. 2010 Dynamics of steep two-dimensional gravity–capillary solitary waves. *J. Fluid Mech.* **664**, 466–477.

NICHOLLS, D. P. 2007 Boundary perturbation methods for water waves. *GAMM-Mitt* **30** (1), 44–74.

PĂRĂU, E. I., VANDEN-BROECK, J.-M. & COOKER, M. J. 2005 Nonlinear three-dimensional gravity–capillary solitary waves. *J. Fluid Mech.* **536**, 99–105.

RYPDAL, K. & RASMUSSEN, J. J. 1988 Stability of solitary structures in the nonlinear Schrödinger equations. *Phys. Scr.* **40**, 192–201.

https://doi.org/10.1017/jfm.2012.320 Published online by Cambridge University Press

SAFFMAN, P. G. 1985 The superharmonic instability of finite-amplitude water waves. *J. Fluid Mech.* **159**, 169–174.

SULEM, C. & SULEM, P. L. 1999 *The Nonlinear Schrödinger Equation: Self-Focusing and Wave Collapse*, *Applied Mathematical Sciences*, vol. 139. Springer.

VANDEN-BROECK, J.-M. & DIAS, F. 1992 Gravity–capillary solitary waves in water of infinite depth and related free-surface flows. *J. Fluid Mech.* **240**, 549–557.

WRIGHT, J. W. 1978 Detection of ocean waves by microwave radar: the modulation of short gravity–capillary waves. *Boundary-Layer Meteorol.* **13**, 87–105.

ZAKHAROV, V. E. 1968 Stability of periodic waves of finite amplitude on the surface of a deep fluid. *J. Appl. Mech. Tech. Phys.* **2**, 190–194.

ZAKHAROV, V. E. 1972 Collapse of Langmuir waves. *Sov. Phys. JETP* **35** (5), 908–914.

ZHANG, X. 1995 Capillary–gravity and capillary waves generated in a wind wave tank: observations and theory. *J. Fluid Mech.* **289**, 51–82.

https://doi.org/10.1017/jfm.2012.320 Published online by Cambridge University Press